Tanzania Journal of Science 50(2): 387-396, 2024
ISSN 0856-1761, e-ISSN 2507-7961

Diffusion-Steered Algorithm for Improving Quality of Images Generated by Electrical Capacitance Tomography Measurement System

George Nyotoka, Nassor Ally*and Josiah Nombo
Electronics and Telecommunications Engineering Department,
University of Dar es Salaam, Tanzania
Received 2 March 2024, Revised 14 May 2024, Accepted, Published June 2024
*naskindy@gmail.com, nassorkindy@udsm.ac.tz
https://dx.doi.org/10.4314/tjs.v50i2.17

Abstract

Electrical Capacitance Tomography (ECT) is a non-invasive, non-intrusive, radiation-free, robust, and cost-efficient measurement system that generates cross-sectional images of industrial operations by measuring differences in dielectric properties within a container. Despite its advantages, the poor quality of reconstructed images limits its applicability. Researchers have explored both non-iterative and iterative methods to address this issue, yet the resulting image quality remains insufficient for high-stakes applications where accurate decision-making is critical. This study proposes a novel algorithm that integrates the ECT model with a diffusion-steered image denoising functional, enhancing the quality of ECT reconstructed images beyond existing methods. Empirical comparisons show that the proposed algorithm outperforms state-of-the-art techniques such as Linear Back Projection and Projected Landweber, with Distribution Error (DE) and Correlation Coefficient (CC) improvements of 62% and 19%, respectively. Qualitative assessments further indicate the superior performance of the proposed algorithm in reconstructing high-quality images.

Keywords: Electrical Capacitance Tomography; Inverse Problem; Image Reconstruction; Diffusion-Steered; Perona-Malik.

Introduction

Tomography is a non-invasive imaging technique that generates a cross-sectional image of an object under observation. It is widely used in industrial process monitoring and medical imaging applications (Murphy et al. 2022). It is can be categorized into two groups, namely hard-field and soft-field tomography. In hard field tomography, the direction of travel of energy waves from the power source is constant, regardless of the type of material or medium. Examples of hard field tomography are X-ray, magnetic resonance imaging, and positron emission (Kure et al. 2021). In soft field tomography, the direction of energy waves is determined through the physical properties of the material being imaged (Sack 2022). Examples of soft field tomography are electrical resistance, electrical capacitance, and electrical impedance (Chowdhury et al. 2022). The choice of using a specific tomography technique in industrial applications depends on the nature of the process being monitored, the desired information from the process, the size of the vessel/pipe, and the environment surrounding the process operation (Khan et al. 2022). Because of the complex nature of industrial processes, measurement and control techniques are essential to improve product quality, simplify processes, and increase efficiency. In the past four decades, tomography measurement systems have played a better role in estimating the process state for better process control (Withers et al. 2021). The implementation of industrial tomography systems can be achieved through

various techniques. However, many techniques are based on measuring electrical properties through the use of capacitive, conductive, and inductive materials under investigation (Zhu et al. 2020). Variation in the electrical properties of different flow components provides process measurement and imaging capabilities using electrical tomography systems (Nombo et al. 2021) The increased interest in electrical tomography techniques for process applications has been motivated by their low construction cost, high speed, safety, and suitability for various sizes of vessels (Rodgers et al. 2021). However, the relatively low resolution of reconstructed images, nonlinearity, and ill posedness of system equations pose a major challenge when dealing with electrical tomography systems (Brazey et al. 2022).

Among the members of the electrical tomography family, Electrical Capacitance Tomography is the most popular in industrial applications. It is a non-invasive and non-destructive imaging technique used in industrial process monitoring and evaluation. ECT technology is highly effective in viewing the cross-sectional material distribution of industrial processes under observation. Compared to other computed tomography techniques, ECT is safer and presents several advantages, such as portability, non-invasiveness, rapid data acquisition, and cost-effectiveness in image reconstruction (Jing et al. 2022).

Many reconstruction methods have been developed to address the above-mentioned problems. The two most popular categories of algorithms are Iterative methods and non-iterative methods or back projection techniques (BP) (Tao et al. 2023). The BP approach produces images of the lowest quality at a minimum computational cost compared to iterative methods (Hussain et al. 2023), which produce images of remarkable quality but the computational cost is very high, which makes both methods not suitable for real-time monitoring of industrial processes. Within these two categories, numerous methods have been proposed by researcher in the last four decades to address the above-mentioned challenges. These methods include Linear back projection, Singular value decomposition, Tikhonov regularization, Landweber iterations, simulated annealing, compressed sensing principle, population entropy, adaptive differential evolution, least-squares methods, support vector machines, self-adaptive particle swarm optimization, fuzzy mathematical modelling, generic algorithms, artificial neural networks, generalized vector sampled pattern matching, total variation regularization, and regularized total least squares (Zhang et al. 2021).

Among these methods Linear back projection was the first method to be applied in ECT, it has a high reconstruction speed but introduces large errors in the generated image (Li et al. 2023). The standard Tikhonov regularization is excellent in solving the ill-posed problem, but generate a smooth approximation solution which leads to the loss of detailed information and results in a low image spatial resolution (He and Hu 2023). Landweber iteration has good image reconstruction quality. However, it has the semi convergence characteristics and is hence not suitable for online imaging environments (Liu and Wang 2022). Optimization methods based on artificial neural networks and genetic algorithms have also been investigated, in these methods the ECT inverse solution is computed by optimizing a set of objective functions to get an estimated solution. The implementation of these methods needs a large set of training data and sometimes they prematurely converge to the solution (Fu et al. 2022).

This work proposes a new image reconstruction method which integrates a diffusion-steered functional that uses the modified Perona-Malik model (Ally et al. 2021) within the sensitivity matrix of the ECT model to address the nonlinearity and ill-posedness challenges. The modified Perona-Malik functional acts as a regularizer and also, provide an anisotropic diffusion mechanism. Empirical comparisons show that the proposed algorithm outperforms state-of-the-art techniques such as Linear Back Projection and Projected Landweber, with Distribution Error (DE) and Correlation

Coefficient (CC) improvements of 62% and 19%, respectively. Qualitative assessments further indicate the superior performance of the proposed algorithm in reconstructing high-quality images.

The ECT system

Electrical Capacitance Tomography (ECT) is a technique that is used to determine the distribution of the constituents of a container or closed pipeline by tracking the differences in the dielectric properties of the material inside the container. This technique is considered to be harmless because it is non-invasive, easily movable, has fast data collection and has low implementation cost as compared to other technologies like X-rays (Qureshi et al. 2021). The ECT system consists of main three components: a multi-electrode sensor, the sensing electronics circuit for data acquisition and a computer system for image reconstruction, data storage, interpretation and display (Figure 1).

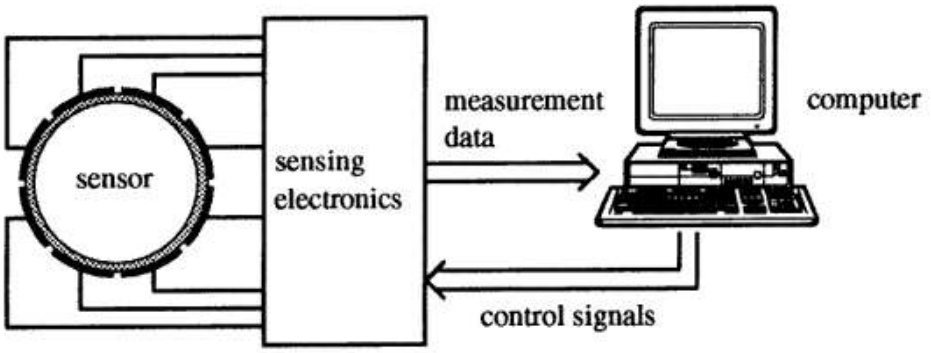

Figure 1: A block diagram of ECT measurement system

The ECT sensor consists of several electrodes, which are mounted around the process being monitored. A sensor with n electrodes contains $n(n-1)/2$ possible combinations of electrode pairs and, therefore, $n(n-1)/2$ independent measurements of capacitance (Korek et al. 2024). The sensor electronics provide an electronic interface between the ECT sensor head and the image reconstruction unit, thus enabling the ECT sensor to interrogate the target process. The image reconstruction unit is a computer that controls the system and implements the associated methods.

ECT image reconstruction techniques

There are three fundamental computational methods for image reconstruction. This includes analytic methods which are considered to be fast, based on exact mathematical answers to the equation in the image (Kaur et al. 2021). However, there is no clear equation that connects the measured capacitances to the permittivity distribution of different components this implies that analytical approaches cannot be used to perform image reconstruction in ECT (Fabijańska and Banasiak 2021). Direct numerical are other methods that use one-step computation, image creation takes a short time but there is an issue with accuracy.

Regularly, these methods are combined with other iterative methods for better image reconstruction. Sometimes, they are used as the initial version of other methods. The iterative methods utilize multiple stages of iteration to address the issue of better-quality images for ECT. It involves solving the forward and inverse problems. The main function or task of the ECT forward problem is to utilize a specific mathematical model to determine the boundary conditions (Hampel et al. 2022) which are applicable in light of the permittivity of the medium that is measured either a container/pipeline or the

parameter of the ECT equipment. The value of capacitance between the electrode pairs in the ECT system is finally attained by calculating a sensitivity map matrix. Among the steps of solving the forward problem is to recalculate new capacitance values based on the permittivity values of the present image vector. Besides, recalculating the sensitivity matrix is a compulsory step in each iteration of the nonlinear technique (Deabes and Amin 2020).

The inverse problem involves the computation of the sensitivity distribution or grey-level values from the calculated capacitance values (Yang et al. 2023). When this inverse problem is solved, it implies that the reconstruction process is performed and is called image reconstruction.

There are two fundamental computational challenges for the ECT image reconstruction, namely the forward problem and the inverse problem. With a predefined permittivity distribution, the potential distribution is calculated by the forward problem so that capacitance measurements can be obtained. The available measured capacitance values obtained can then be used to compute permittivity, and this is achieved by solving the inverse problem. Therefore, the process is named image reconstruction because the final result of the inverse problem is an image in grey-level format. Equation (1) shows a relationship between capacitance and permittivity distribution.

$$C = -\frac{1}{V}\iint_{\tau}\varepsilon(x,y)\nabla\emptyset(x,y)d\tau, \quad (1)$$

Where τ is the electrode surface, $\varepsilon(x,y)$ and $\phi(x,y)$ are respectively, permittivity and potential distribution, and V is the potential difference between electrode pair forming capacitance.

ECT Diffusion-Steered Method

The Perona-Malik (PM) algorithm (equation (2)) was thoroughly investigated prior to designing the diffusion-steered functional. The PM algorithm aims to remove noise from an image while preserving significant edges, which are crucial for image interpretation. This method uses image content to control the diffusion process, preventing diffusion at edges and thereby preserving them. The PM diffusion coefficient, which is high in areas without edges and low at edges, serves as the foundation for the diffusion-steered functional.

$$\frac{\partial u}{\partial t} = div\left(\frac{1}{1+\left(\frac{|\nabla u|}{K}\right)^2}\nabla u\right) - \lambda(u-f) \quad (2)$$

Where K is the tuning constant which is sensitive to edges, u is the most recent cleaned image intensity after n iteration while f is an image intensity in an (*n-1*) iteration, λ is a fidelity parameter that controls a tradeoff between *u* and *f*, *t* is the time (iteration step), ∇u is an image gradient Designing of The Diffusion-Steered Functional was done by considering the exponential combinations of m and n in equation (3) which provides a high-quality image with preserved edge content.

$$\frac{\partial u}{\partial x} = div\left(\frac{1}{1+\left(\frac{(|\nabla u|)^m}{(u_\epsilon)^n}\right)}\nabla u\right) - \lambda\left(\frac{u-f}{u_\epsilon^{\frac{1}{\propto}}}\right) \quad (3)$$

Where λ defines the regularization parameter.

Through a series of tests conducted on reconstructed textured and natural images, it was discovered that $m = 6$ and $n = 3$ yield better outcomes. Various combinations of m and n values were tested, ranging from low to high, followed by visual assessments. The combination of $(6,3)$ was chosen because it consistently produced higher quality indices across the different evaluated images. Equation (4) was derived by inserting $(m,n) = (6,3)$ into theoretical equation (3).

$$\frac{\partial u}{\partial x} = div\left(\frac{1}{1+\left(\frac{(|\nabla u|)^6}{(u_\epsilon)^3}\right)}\nabla u\right) - \lambda\left(\frac{u-f}{u_\epsilon^{\frac{1}{\propto}}}\right) \quad (4)$$

which can also be rewritten as

$$\frac{\partial u}{\partial x} = div\left(\frac{1}{1+\left(\frac{|\nabla u|^2}{u_\epsilon}\right)^3}\nabla u\right) - \lambda\left(\frac{u-f}{u_\epsilon^{\frac{1}{\propto}}}\right). \quad (5)$$

Equation (5) provides the suggested model's desired performance—higher PSNR, MSSIM, and aesthetically pleasing images. The evolving image in this equation, represented by (u), approaches the initial

(clean) image as time (t) gets closer to infinity. Deriving λ from equation (6), we can deduce the regularization parameter as follows;

$$\lambda = \frac{1}{|\Omega| v^2} \int_{\Omega} \left(1 - \frac{f}{u}\right) \left[div \left(\frac{1}{1 + \left(\frac{|\nabla u|^2}{u_{\epsilon}}\right)^3} \nabla u \right) \right] \quad (6)$$

The developed diffusion functional based on the Perona-Malik (PM) diffusion coefficient, a diffusion-steered functional, was incorporated into the ECT reconstruction model as presented in the following steps.

Firstly, the ECT algorithm was modified with a series of experiments to come up with a new regularization parameter that enhanced the spatial resolution of the reconstructed ECT images. The least-square form of the ECT model given in Equation (7); was used to come up with an equation for G. In this equation C is the normalized capacitance vector, S is the sensitivity matrix of normalized capacitance concerning permittivity distribution, and G is the grey-level vector.

$$G = (S^T S)^{-1} S^T C \quad (7)$$

From equation (7), G can be calculated as;

$$G = (S^T S)^{-1} S^T C \, (8)$$

From the equation (8), $S^T S$ is a non-invertible matrix, and when a regularization parameter is introduced, it becomes;

$$G = (S^T S + \mu I)^{-1} S^T C \quad (9)$$

where I is the identity matrix and μ is the regularization parameter. The value of the regularization parameter greatly affects how well the reconstructed images turn out. A moderate value of the regularization parameter yields a good estimate of the permittivity distribution, still, the solution is significantly impacted by the capacitance measurement's inaccuracy. Furthermore, the capacitance error increases but the approximation error decreases with a high value of the regularization parameter. By combining the modified PM equation (6) and the ECT equation (9), we developed a new model, resulting in equation (10).

$$G = \left(S^T S + \left(\frac{1}{|\Omega| v^2} \int_{\Omega} \left(1 - \frac{f}{u}\right) \left[div \left(\frac{1}{1 + \left(\frac{|\nabla u|^2}{u_{\epsilon}}\right)^3} \nabla u \right) \right] \right) I \right)^{-1} S^T C \quad (10)$$

The benefit of the proposed model lies in its ability to generate high-quality images, which offer several advantages. These images will enable accurate monitoring, providing operators with precise data for effective control and monitoring of industrial processes. High quality images also, will facilitate efficient parameter optimization during industrial process operations. Additionally, the ability to detect abnormalities early will allow timely interventions to prevent hazards or accidents and minimize equipment downtime. This improvement in operational efficiency will reduce the need for extensive maintenance, hence enhancing overall reliability. Moreover, from a research perspective, the reconstructed images will support advanced activities in industrial process control and monitoring.

Experimental Setup and Evaluation Criteria

To validate the efficacy of the ECT diffusion steered-based algorithm experiments were carried out using an 8-electrode circular sensor ECT system (excitation waveform: 10Vpp, 300-500kHz), with a sensing domain divided into 900 pixels with 32 ×32 grid. Static experiments were conducted using annular and stratified perspex beads positioned at different locations in the sensing domain. Simulated capacitance data were used to analyze the performance of the proposed method over the full component fraction range. All reconstruction methods were implemented using MATLAB on a computer with Intel Core i7-4510U CPU, @ 2 GHz, 2GHz, and 8.00GB memory. These methods include Landweber iteration (LAND), projected Landweber iteration (PLAND) and Linear back projection (LBP).

Both qualitative and quantitative evaluations of denoised images were

performed using both existing and proposed algorithms. Visual evaluation was used to assess qualitatively how well the algorithms preserved the texture and edges of the maps during image reconstruction. DE and CC are the metrics used in evaluating and validating the efficacy of the algorithm against the state-of-the-art methods.

Distribution Error (DE): is obtained by computing a total sum of the average of absolute difference in grey lever values between the reference image and reconstructed. Equation (11) is a formula that shows how the Distribution Error DE is calculated.

$$DE = \frac{1}{n}\sum_{i=1} \left| G_i^{yeC} G_i^{ref} \right| \qquad (11)$$

Where n is the total number of grey levels. G_i^{yeC}

Correlation Coefficient (CC): Between the reference image and the reconstructed image The calculation formula of the correlation coefficient (CC) is as shown in Equation (12).

$$CC = \frac{\sum_{e=1}^{M} \left(G_i^{rec} - \underline{G_i^{rec}}\right)\left(G_i^{ref} - \underline{G_i^{ref}}\right)}{\sqrt{\sum_{e=1}^{M} \left(G_i^{rec} - \underline{G_i^{rec}}\right)^2 \sum_{e=1}^{M} \left(G_i^{ref} - \underline{G_i^{ref}}\right)^2}} \qquad (12)$$

where G_i^{rec} *and* $\underline{G_i^{ref}}$ are, respectively, reconstructed and reference image vectors.

The best results from the system should have lower values of RIE and DE, and a higher CC.

Results and Discussion

Figure 2 presents a qualitative evaluation of the proposed method compared to Linear back Projection (LBP) and Projected Landweber (PLAND) methods. The reconstructions are based on actual capacitance measurements of dielectric objects located at different positions of the sensing domain. Each row contains a reference image, and reconstructions using LBP, Projected Landweber and the Proposed Method. Results show an improvement in the quality of images generated using the proposed method compared with those of LBP and PLAND for all seven test objects. However, the proposed method fails to reconstruct bubble flows, unless thresholding is applied. The evaluation was extended to assess the qualitative performance for annular and stratified flows.

Figure 3 presents the Distribution Error (DE) results which are used to assess how accurately reconstructed images match their reference image counterparts across different methods: The DE values for Linear Back Projection (LBP), PLAND, and the Proposed Method are presented graphically as percentage, highlight the effectiveness of each method in minimizing errors between reconstructed and original images.

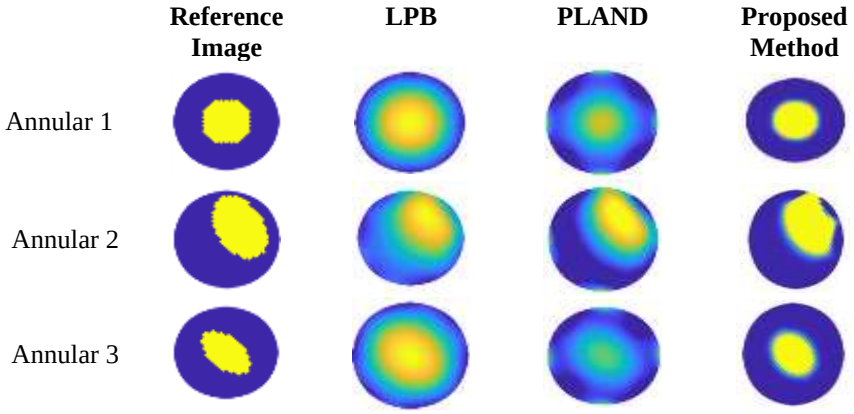

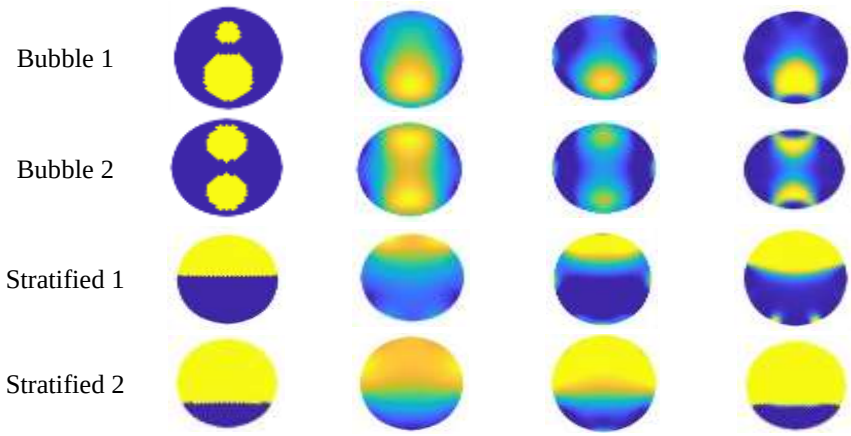

Figure 2: Image reconstructed from experiment data

For different types of flows, such as Annular, Bubble, and Stratified, the Proposed Method consistently exhibits notable reductions in DE compared to LBP and PLAND. For instance, in Annular images, DE reductions of 2.04%, 6.59%, and 3.92% for Annular 1, Annular 2, and Annular 3, respectively, underscore the Proposed Method's ability to produce images closer to reference images than its counterparts. Similarly, in Bubble images, reductions like 13.67% for Bubble 1 and 17.01% for Bubble 2 demonstrate substantial improvements over LBP and PLAND.

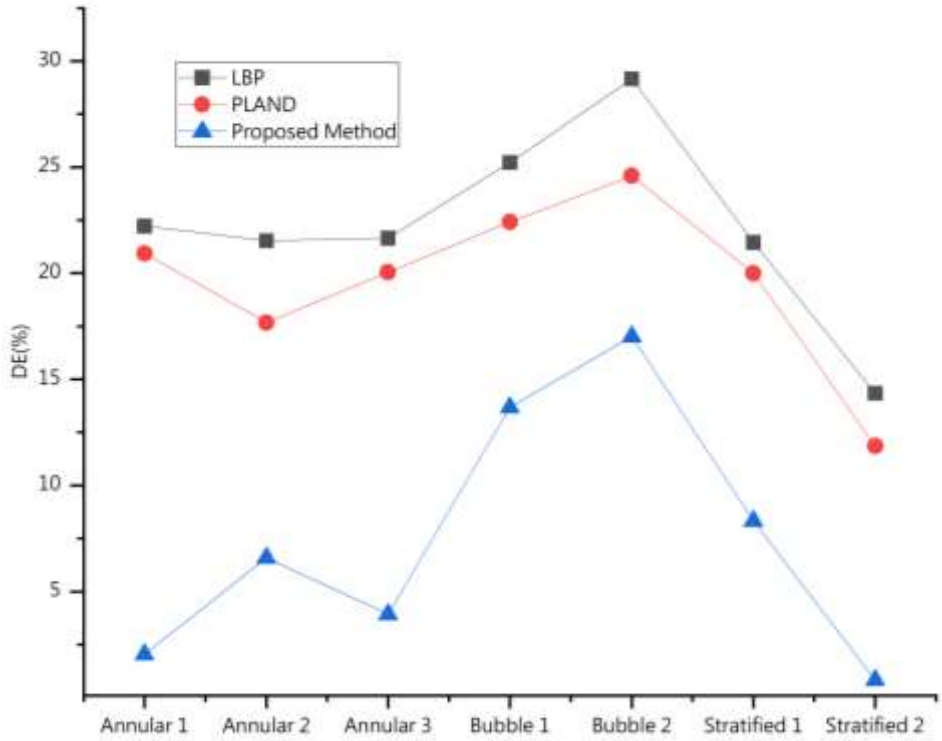

Figure 3: Distribution error (%) for Selected Reconstructed Images

Figure 3 shows Correlation Coefficient (CC) results, which measures the degree of similarity between reconstructed images and reference images. Higher CC values indicate stronger correlations and better fidelity to the original images. The results in Figure 3 reveal that the Proposed Method consistently achieves higher CC values compared to LBP and PLAND across all types of reconstructed images. This suggests that not only does the Proposed Method reduce Distribution Error (DE), but it also maintains a high level of similarity (CC) with the reference images, indicating superior image quality and fidelity.

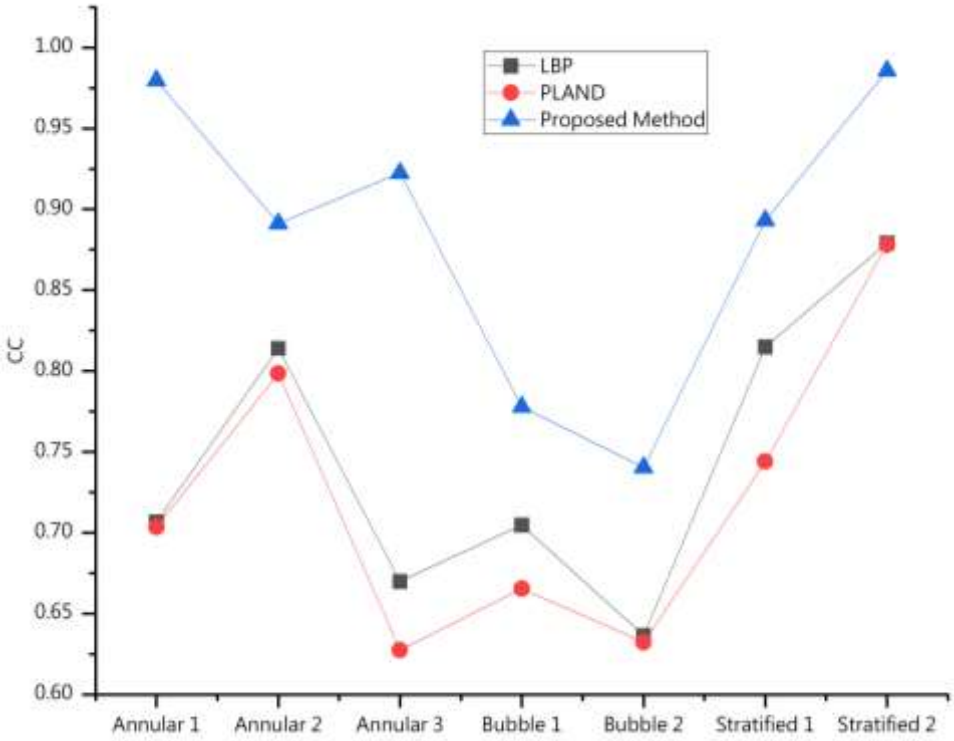

Figure 4: Correlation Coefficient for Selected Reconstructed Images

In general, Figures 3 and 4 collectively demonstrate that the Proposed Method outperforms LBP and PLAND in both reducing Distribution Error (Figure 3) and maintaining high Correlation Coefficients (Figure 4). These findings validate the effectiveness of the Proposed Method in enhancing the visual quality and accuracy of reconstructed images in various practical applications, including industrial monitoring and research activities in materials fabrication and process monitoring.

Conclusion

In conclusion, the proposed algorithm demonstrates substantial improvements in image reconstruction quality. By combining the ECT model with the modified Perona-Malik functional, the algorithm effectively addresses the challenges of nonlinearity and ill-posedness, yielding superior image quality compared to traditional methods such as Linear Back Projection (LBP) and Projected Landweber (PLAND). Experimental results indicate significant improvements in both Distribution Error and Correlation Coefficient, confirming the superior performance of the proposed method. These advancements hold considerable promise for improved industrial process monitoring and more accurate decision-making in high-stakes applications.

References

Ally N, Nombo J, Ibwe K, Abdalla AT, and Maiseli BJ 2021 Diffusion-Driven Image Denoising Model with Texture Preservation Capabilities. *J. Sign. Process. Syst*. 93(8): 937–949.

Brazey B, Haddab Y, and Zemiti N 2022 Robust imaging using electrical impedance tomography: review of current tools. *Proc. R. Soc. A*. 478(2258).

Chowdhury SM, Marashdeh Q, Teixeira FL, and Fan LS 2022 Electrical Capacitance Tomography. *Indust. Tomogr.: Syst. Appl. 2nd Ed*. 3–29.

Deabes W and Amin HH 2020 Image reconstruction algorithm based on PSO-tuned fuzzy inference system for electrical capacitance tomography. *IEEE Access*. 8: 191875–191887.

Fabijańska A and Banasiak R 2021 Graph convolutional networks for enhanced resolution 3D Electrical Capacitance Tomography image reconstruction. *Appl. Soft Comput*. 110: 107608.

Fu W, Wang M, He X, Hao S, and Wu X 2022 A Survey on Large-Scale Machine Learning. *IEEE Trans. Knowl. Data Engin*. 34(6): 2574–2594.

Hampel U, Babout L, Banasiak R, Schleicher E, Soleimani M, Wondrak T, Vauhkonen M, Lähivaara T, Tan C, Hoyle B, et al. 2022 A Review on Fast Tomographic Imaging Techniques and Their Potential Application in Industrial Process Control. *Sensors* 22(6): 2309.

He C and Hu C 2023 Ill-Poseness of Imaging Inverse Problems and Regularization for Detail Preservation 51–72.

Hussain A, Faye I, Muthuvalu MS, Tang TB, and Zafar M 2023 Advancements in Numerical Methods for Forward and Inverse Problems in Functional near Infra-Red Spectroscopy: A Review. *Axioms* 12(4): 326.

Jing J, Liu S, Wang G, Zhang W, and Sun C 2022 Recent advances on image edge detection: A comprehensive review. *Neurocomputing*. 503: 259–271.

Kaur M, Singh S, and Kaur M 2021 Computational Image Encryption Techniques: A Comprehensive Review. *Math. Probl. Engin*. 2021(1): 5012496.

Khan MA, Yousaf MZ, Zain Yousaf M, Mustafa A, Ullah R, and Baig MB 2022 Future Maintenance Effects on Life Cycle of Large Above Storage Tanks and Improvements.

Korek E-M;, Teotia R;, Herbig D;, Brederlow R, Korek E-M, Teotia R, Herbig D, and Brederlow R 2024 Electrochemical Impedance Spectroscopy for Ion Sensors with Interdigitated Electrodes: Capacitance Calculations, Equivalent Circuit Models and Design Optimizations. *Biosensors* 14(5): 241.

Kure AJ, Savas H, Hijaz TA, Hussaini SF, and Korutz AW 2021 Advancements in Positron Emission Tomography/Magnetic Resonance Imaging and Applications to Diagnostic Challenges in Neuroradiology. *Seminars in Ultrasound, CT and MRI*. 42(5): 434–451.

Li J, Tang Z, Zhang B, and Xu C 2023 Deep learning-based tomographic imaging of ECT for characterizing particle distribution in circulating fluidized bed. *AIChE J.*. 69(5): e18055.

Liu X and Wang Y 2022 An Improved Conjugate Gradient Image Reconstruction Algorithm for Electromagnetic Tomography. *Sens. Imaging*. 23(1): 1–19.

Murphy CT, Müller R, and Jung S 2022 Sample digitization techniques for bio-inspired engineering. *Biomim. Mater. Design Habitats: Innov. Appl.* 215–246.

Nombo J, Mwambela A, and Kisangiri M 2021 Analysis and Performance Evaluation of Entropic Thresholding Image Processing Techniques for Electrical Capacitance Tomography Measurement System. *Tanz. J. Sci*. 47(3): 928–942.

Qureshi MF, Ali MH, Ferroudji H, Rasul G, Khan MS, Rahman MA, Hasan R, and Hassan I 2021 Measuring solid cuttings transport in Newtonian fluid across horizontal annulus using electrical resistance tomography (ERT). *Flow Measure. Instrum.* 77: 101841.

Rodgers T, Lionheart W, and York T 2021 Industrial process tomography. *Electric. Imped. Tomogr.: Methods Hist. Appl*.

403–422.

Sack I 2022 Magnetic resonance elastography from fundamental soft-tissue mechanics to diagnostic imaging. *Nat. Rev. Phys. 2022 5:1*. 5(1): 25–42.

Tao J, Ni W, Song C, and Wang X 2023 FSSBP: Fast Spatial–Spectral Back Projection Based on Pan-Sharpening Iterative Optimization. *Remote Sens.* 15(18): 4543.

Withers PJ, Bouman C, Carmignato S, Cnudde V, Grimaldi D, Hagen CK, Maire E, Manley M, Du Plessis A, and Stock SR 2021 X-ray computed tomography. *Nat. Rev. Methods Prim. 2021 1:1*. 1(1): 1–21.

Yang Y, Liu J, and Liu G 2023 Image reconstruction for ECT based on high-order approximate sensitivity matrix. *Measure. Sci. Technol*. 34(9): 095402.

Zhang S, Wang Y, Jiang J, Dong J, Yi W, and Hou W 2021 CNN-Based Medical Ultrasound Image Quality Assessment. *Complex*. 2021.

Zhu S, Huang R, Salas Avila JR, Tao Y, Zhang Z, Zhao Q, Peyton AJ, and Yin W 2020 Simultaneous Measurements of Wire Diameter and Conductivity Using a Combined Inductive and Capacitive Sensor. *IEEE Sens. J*. 20(19): 11617–11624.